Annals of Hepatology 30 (2025) 101776

Contents lists available at ScienceDirect

Annals of Hepatology

journal homepage: www.elsevier.es/annalsofhepatology

Original article

The promoting effect of the POU3F2/METTL16/PFKM cascade on glycolysis and tumorigenesis of hepatocellular carcinoma

Ming Chen[a], Yuan Yang[a], Guangsheng Hu[a], Zhong Peng[b], Wu Wen[c,*]

[a] Department of Gastroenterology and Hepatology, the First Affiliated Hospital, Hengyang Medical School, University of South China, Hengyang City, 421001, Hunan, China
[b] Department of Gastroenterology and Hepatology, Yiyang Central Hospital, Yiyang City, 413099, Hunan, China
[c] Department of Hepato-Biliary-Pancreatic Surgery, the First Affiliated Hospital, Hengyang Medical School, University of South China, Hengyang City, 421001, Hunan, China

ARTICLE INFO

Article History:
Received 22 October 2024
Accepted 17 December 2024
Available online 3 January 2025

Keywords:
Hepatocellular carcinoma
Glycolysis
METTL16
m^{6}A methylation
Transcription factor

ABSTRACT

Introduction and Objectives: Deregulation of m^{6}A methylation, the most prevailing RNA modification, participates in cancer pathogenesis. METTL16, an atypical methyltransferase, functions as a pro-tumorigenic factor in hepatocellular carcinoma (HCC). Here, we explored the action of METTL16 on HCC glycolysis and the associated mechanism.

Materials and Methods: Expression analysis was done by quantitative PCR, immunoblotting, or immunohistochemistry. Cell sphere formation, invasiveness, apoptosis, proliferation and viability were detected by sphere formation, transwell, flow cytometry, EdU and CCK-8 assays, respectively. Xenograft studies were performed to analyze the role *in vivo*. Methylated RNA immunoprecipitation (MeRIP) and RIP assays were used to verify the METTL16/PFKM relationship. *PFKM* mRNA stability was tested by actinomycin D treatment. Chromatin immunoprecipitation (ChIP) and luciferase assays were performed to analyze the POU3F2/*METTL16* relationship.

Results: In HCC, METTL16 expression was elevated, and increased levels of *METTL16* transcript predicted poor HCC prognosis. METTL16 deficiency resulted in suppressed HCC cell growth, invasiveness and sphere formation. Moreover, METTL16 depletion diminished HCC cell glycolysis. Mechanistically, PFKM expression was positively associated with METTL16 expression. METTL16 mediated m6A methylation to stabilize *PFKM* mRNA via an IGF2BP3-dependent manner. Restored PFKM expression exerted a counteracting effect on METTL16 deficiency-mediated *in vitro* cell phenotype alterations and *in vivo* xenograft growth suppression. Furthermore, POU3F2 promoted the transcription of *METTL16* in HCC cells.

Conclusions: Our findings define the crucial role of the POU3F2/METTL16/PFKM axis in HCC pathogenesis, offering the potential opportunity to combat HCC.

1. Introduction

Liver cancer leads to more a million cancer-associated deaths (7.8 % of the total cancer deaths) throughout the world in 2022 and has become the third predominant determinant of cancer mortality, with hepatocellular carcinoma (HCC) accounting for 75–85 % of all cases [1]. The etiology of HCC is closely linked to multiple factors, such as hepatitis virus infection, chronic liver disease, and gene susceptibility [2]. Despite the advantage of advances of systemic therapies in the early stage, HCC remains terrible survival because it is often confirmed at an advanced stage [2,3]. Currently, studies exploring the molecular pathogenesis of HCC are needed to devise novel markers for HCC diagnosis and management at all stages. Enhanced glycolysis can facilitate cancer cell survival and contribute to pro-cancerous tumor environment. Targeting glycolysis has been proposed to be useful for the improvement of HCC therapy [4].

Deregulation of m^{6}A methylation, the most prevailing RNA modification in eukaryotes, has been reported in human cancer [5]. m^{6}A modification is controlled by methyltransferases (m6A writers), demethylases (m6A erasers) and m6A binding proteins (m6A readers). METTL16, a member of methyltransferase complex, is capable of functioning as an atypical methyltransferase to catalyze RNA m6A methylation, thereby actively participating in cancer pathogenesis [6]. For instance, METTL16-mediated m6A modification contributes to leukemogenesis by affecting branched-chain amino acid (BCAA)

Abbreviations: BCAA, branched-chain amino acid; ChIP, Chromatin immunoprecipitation; DEGs, differentially expressed genes; HCC, hepatocellular carcinoma

* Corresponding author.
E-mail address: wenwu2023ww@163.com (W. Wen).

https://doi.org/10.1016/j.aohep.2025.101776

metabolism by upregulating the levels of BCAA transaminase 1 and 2 [7]. METTL16 enhances *cyclin D1* mRNA m6A modification to stabilize the transcript, thus leading to enhanced proliferation of gastric cancer cells [8]. The pro-tumorigenic role of METTL16 in HCC has begun to emerge; for example, METTL16 accelerates HCC development by affecting the stabilization of *RAB11B-AS1* transcript via an m6A mechanism [9]; METTL16 mediates m6A methylation of *Lnc-CSMD1–7* to induce HCC metastasis [10]. Nonetheless, our understanding of the action of METTL16 on HCC glycolysis and its associated mechanism has remained incomplete.

In the current work, our data show new evidence for the pro-tumorigenic role of METTL16 in HCC. We further demonstrate the promoting activity of METTL16 in HCC glycolysis. Through bioinformatic and experimental analyses, we elucidated an uncharacterized associated mechanism, providing a novel foundation for targeting METTL16 as an encouraging target for HCC management.

2. Materials and Methods

2.1. Bioinformatics

The previously developed ENCORI algorithm (https://rnasysu.com/encori/) was used to observe the expression pattern of *METTL16* transcript in HCC, to reveal the expression correlation of *PFKM* with *METTL16* or *IGF2BP3* in HCC, and to predict m6A readers associated with *PFKM* mRNA. The open-access TCGA database (https://www.cancer.gov/ccg/research/genome-sequencing/tcga) was used for analysis of *PFKM* or *IGF2BP3* transcript expression in HCC. To evaluate the association of HCC overall survival with *METTL16, IGF2BP3* or *PFKM* expression, the online tool Kaplan-Meier Plotter was used at https://www.kmplot.com/analysis/. We applied the human protein atlas online resource (https://www.proteinatlas.org/) to analyze METTL16 protein expression in HCC. The GSE224008 dataset on NCBI (https://www.ncbi.nlm.nih.gov/) was applied to reveal differentially expressed genes (DEGs) after METTL16 silencing in Huh-7 liver cancer cells, and these DEGs were subjected to KEGG pathway enrichment analysis at https://www.bioinformatics.com.cn/?keywords=pathway. We used the online website SRAMP to predict the putative m6A methylation sites of *PFKM* mRNA at http://www.cuilab.cn/sramp. To search for the transcription factors (TFs) in promoting *METTL16* transcription, we utilized three TF-predicting algorithms Genecards (https://www.genecards.org/), PROMO (https://alggen.lsi.upc.es/cgi-bin/promo_v3/promo/promoinit.cgi?dirDB=TF_8.3) and JASPAR (https://jaspar.elixir.no/). The JASPAR algorithm was also used to predict the putative binding sites for POU3F2 in the *METTL16* promoter.

2.2. Human tissue specimens

In this study, we obtained fresh-frozen human primary HCC tumors (n = 40) and matched non-cancerous tissues (n = 40) from HCC patients from the First Affiliated Hospital, Hengyang Medical School, University of South China, after acquisition of patients' informed consent. Clinical follow-up ranged from 6 to 60 months. Human research protocols were authorized by the First Affiliated Hospital, Hengyang Medical School, University of South China Ethics and Scientific Committee. In accordance with the standard guidelines, we extracted total RNA and protein from these specimens.

2.3. mRNA expression by quantitative PCR

Using the BeyoMag™ RNA Kit and accompanying suggestions (Beyotime, Shanghai, China), we prepared total RNA from human tissues. 500 ng of RNA was subjected to reverse transcription using the QuantiTect RT Kit as per the manufactory suggestions (Qiagen, Tokyo, Japan). To gauge the levels of *POU3F2, METTL16*, and *PFKM* transcripts, quantitative PCR was done following cDNA generation under the application of SYBR Green mix (Takara, Dalian, China) and gene-specific primers (Table 1). For relative quantification analysis, *GAPDH* served as a reference gene, and the $2^{-\Delta\Delta Ct}$ method was used.

Table 1
Primers sequences used for quantitative PCR.

Name		Primers for PCR (5′–3′)
METTL16	Forward	GGGAGCGTATCATCTGCGTT
	Reverse	AGTCAGGAGGTTTGTCCTTGT
PFKM	Forward	GGCGGAGGAGAGCTAAGACTA
	Reverse	TACCAACTCGAACCACAGCC
POU3F2	Forward	TTGTGTTGCCCCTTCTTCGT
	Reverse	TTGCCTTCGATAAAGCGGGT
GAPDH	Forward	AGAAGGCTGGGGCTCATTTG
	Reverse	AGGGGCCATCCACAGTCTTC

2.4. Cell lines

This study included MHCC97 (#C6585, Beyotime), Huh-7 (#IM-H040, Immocell, Xiamen, China), and Hep3B HCC cells (#IM-H367, Immocell) and THLE-2 cells (#CL-0833, Procell, Wuhan, China). For cell cultivation (MHCC97, Huh-7, Hep3B), we utilized the complete medium consisted of 89 % DMEM, 10 % FBS and 1 % streptomycin/penicillin (all from Beyotime). THLE-2 cells were propagated in Human liver immortalized cell growth media purchased from Procell. A humidified 5 % CO_2 incubator (Thermo Fisher Scientific, Geel, Belgium) was used for cell culture at 37 °C.

2.5. SiRNAs, plasmids, lentivirus particles, transfection, and transduction

This study used the following siRNAs (MedChemExpress, Shanghai, China): si-METTL16#1, si-METTL16#2, si-METTL16#3, si-IGF2BP3, si-YY1, si-POU3F2, and si-NC control. The 1:1 ratio mix of si-METTL16#1 and si-METTL16#3 was named as si-METTL16. pCMV-IGF2BP3(human)−3×FLAG-Neo, pCMV-3×FLAG-PFKM(human)-Neo, and matched control vector were procured from Miaoling Biology (Wuhan, China). Lentivirus particles expressing sh-METTL16 or sh-NC control were from Genomeditech (Shanghai, China).

For transfection, we seeded MHCC97 and Huh-7 HCC cells 18–20 h before transfection to yield 60–75 % confluence at the time of transfection. Using Lipofectamine 3000 as suggested by the supplier (Thermo Fisher Scientific), liposomal cocktails with siRNA or/and plasmid were prepared in Opti-MEM (Thermo Fisher Scientific). Transfection complexes were added into cells, followed by incubation for 8 h before media change. For the further use, we obtained transfected cells that were cultured for 24–72 h.

For viral transduction, we plated 1×10^6 MHCC97 cells into a 10-cm dish 10–12 h prior to infection of sh-METTL16 or sh-NC lentivirus for 18–24 h Following media change, cells were subjected to drug selection (2 μg/mL puromycin) for at least 14 days.

2.6. Animal studies, immunohistochemistry, and H&E staining

Mouse xenograft studies were conducted following protocols approved by the First Affiliated Hospital, Hengyang Medical School, University of South China Animal Care and Use Ethics Committee Hospital. For these studies, we used female BALB/c nude mice (42–56-day old, n = 24, Vital River Laboratory, Beijing, China) and divided them in three groups: sh-NC (n = 8), sh-METTL16 (n = 8), and sh-METTL16+PFKM (n = 8). For subcutaneous xenograft generation, 100 μL of suspension containing 1.5×10^6 lentivirus-infected MHCC97 cells was mixed with 100 μL of Matrigel (BD Biosciences, Stockholm, Sweden) prior to cell implantation in nude mice by subcutaneous injection (n = 5 for each group). For metastasis analysis,

MHCC97 cells were intravenously into nude mice through tail vein injection (n = 3 for each group). Intratumoral or nasal administration of the PFKM expression lentivirus (10^7 TU/mouse) was performed on day 8. Xenograft tumors were gauged every three days by caliper (volume=longest diameter × (shortest diameter)^2 × 0.5) until resected. Mice were used for lung collection (metastatic node quantification) at week 6.

A portion of xenograft tumors were inflated into 4 % paraformaldehyde, embedded in paraffin, sectioned (4–5 μm), and subjected to immunohistochemistry for probing of Ki67 and PFKM as described elsewhere [11], using rabbit anti-Ki67 pAb (#27309-1-AP, Proteintech, Wuhan, China, 1 to 5000) and rabbit anti-PFKM pAb (#ab237545, Abcam, Cambridge, UK, 1 to 150). Mouse lungs were fixed, embedded in paraffin, sectioned (4–5 μm), and subjected to H&E staining using a commercial staining kit (Beyotime).

2.7. Protein analysis by immunoblotting

We obtained total protein from collected tissue specimens or cultured cell lines and performed western blot assays as reported [12]. For immunoblot analysis, we used mouse anti-POU3F2 mAb (#ab243045, Abcam, 1 to 1000), rabbit anti-METTL16 pAb (#19924-1-AP, Proteintech, 1 to 8000), rabbit anti-PFKM pAb (#ab237545, Abcam, 1 to 150), rabbit anti-IGF2BP3 pAb (#14642-1-AP, Proteintech, 1 to 6000), rabbit anti-YY1 mAb (#ab109237, Abcam, 1 to 5000), and mouse anti-β-actin mAb (#ab8226, Abcam, 1 to 1000).

2.8. Cell viability and proliferation assays

In a 96-well plate, MHCC97 and Huh-7 cells were subjected to transfection with si-NC, si-METTL16#1, si-METTL16#3, si-METTL16 (the 1:1 ratio mix of si-METTL16#1:si-METTL16#3), si-METTL16+vector or si-METTL16+PFKM expression plasmid. After 48 h, we utilized the CCK-8 Viability Assay Kit (Yeasen, Shanghai, China) to evaluate the number of viable cells and the EdU incorporation Assay Kit (Ribobio, Guangzhou, China) for cell proliferation analysis as recommended by the vendors. A Multiskan Ascent 354 reader (Thermo Fisher Scientific) was used for absorbance measurement at 450 nm. For fluorescence image acquisition, we utilized the FV3000 confocal microscope (Olympus, Tokyo, Japan).

2.9. Flow cytometry

MHCC97 and Huh-7 cells after 72 h transfection were subjected to staining by the Annexin V-FITC/PI Apoptosis Assay Kit as described by the supplier (BD Biosciences). For FACS analysis, we applied a Calibur flow cytometer with CellQuest software (BD Biosciences).

2.10. Transwell invasion assay

We plated 7×10^4 MHCC97 and Huh-7 cells (in non-serum media) at 24 h post transcription atop each transwell pre-coated with Matrigel (BD Biosciences). 10 % FBS media was used as a chemoattractant in the bottom well. Following incubation for 24 h at 37 °C, the number of the cells remaining on the lower surface was quantified after crystal violet (1 %) staining.

2.11. Sphere formation assay

For the assay, we used a 96-well Clear Round Bottom Ultra Low Attachment plate (Corning, Shanghai, China). We seeded 200 MHCC97 and Huh-7 cells after 24 h introduction into each well in non-serum media. Under standard protocols, cell culture was done for 7 days. We analyzed the efficiency of sphere formation by microscopic images.

2.12. Detection of glucose consumption level, lactate production content, and ATP/ADP ratio

MHCC97 and Huh-7 cells at 48 h post transfection were harvested for these detections. In accordance with the suppliers' suggestions, the glucose consumption Assay Kit (Beyotime) was applied for glucose consumption content measurement, the lactate production Assay Kit (Abcam) was used to gauge lactate production level, and the ATP/ADP ratio Chemiluminescence Assay kit (Elabscience, Wuhan, China) was employed to analyze the ATP/ADP ratio.

2.13. Methylated RNA immunoprecipitation (MeRIP) and RIP assays

Si-METTL16-transfected, si-NC-introduced, and untransfected MHCC97 and Huh-7 cells were subjected to RIP experiments using BeyoRIP^{TM} RIP Assay Kit as recommended by the producer (Beyotime). The complex of Protein A/G Agarose and rabbit anti-m6A mAb (#MA5-33030, Thermo Fisher Scientific), rabbit anti-METTL16 pAb (#A304-192A, Bethyl Laboratories, Lucerne, Switzerland), rabbit anti-IGF2BP3 pAb (#14642-1-AP, Proteintech), or rabbit anti-IgG pAb (#30000-0-AP, Proteintech) was added into the lysates. Following incubation for 6 h at 4 °C, we isolated RNA from the precipitates to assess *PFKM* mRNA enrichment by quantitative PCR.

2.14. Analysis of PFKM mRNA stability

Si-METTL16-transfected or si-NC-introduced MHCC97 and Huh-7 cells were maintained in media containing 50 μg/mL Actinomycin D (Act D, Beyotime). We extracted RNA from treated cells to evaluate *PFKM* mRNA levels at 0, 3, 6 and 9 h thereafter.

2.15. Chromatin immunoprecipitation (ChIP) assay

To validate the relationship of POU3F2 with the *METTL16* promoter, we applied the ChIP Assay Kit (Beyotime) to perform ChIP experiments. Briefly, chromatin DNA was obtained from MHCC97 and Huh-7 cells and then subjected to fragmentation. Protein A/G Agarose and rabbit anti-POU3F2 pAb (#PA5-30124, Thermo Fisher Scientific) or rabbit anti-IgG pAb (#30000-0-AP, Proteintech) was mixed to generate bead-antibody complex, which was added into the suspension of DNA fragments. Following incubation for 8 h at 4 °C, we prepared RNA from the precipitates to detect the enrichment of the *METTL16* promoter segments by quantitative PCR.

2.16. Luciferase reporter assay

We generated METTL16 reporters by cloning the *METTL16* promoter fragment harboring the predicted binding sequence (WT) or mutant target region (MUT) into the pGL3 basic vector (Thermo Fisher Scientific). MHCC97 and Huh-7 cells were co-transfected with WT-METTL16 or MUT-METTL16 and si-NC or si-POU3F2. The pRL-TK plasmid (Promega, Charbonnières, France) was also introduced into cells as the normalized control. At 48 h post transfection, we quantified the luciferase activity using Dual-Luciferase reporter system (Promega).

2.17. Data analysis

We expressed data using mean±SD. For significance comparisons, we used Mann Whitney U test, unpaired t-test or ANOVA (one- or two-way). For survival analysis, we applied the Kaplan-Meier survival accompanied by log rank tests. Values of $P < 0.05$ were significant.

2.18. Ethical statement

Human research protocols were authorized by the First Affiliated Hospital, Hengyang Medical School, University of South China Ethics and Scientific Committee. Mouse xenograft studies were conducted following protocols approved by the First Affiliated Hospital, Hengyang Medical School, University of South China Animal Care and Use Ethics Committee.

3. Results

3.1. METTL16 is upregulated in HCC and its deficiency results in suppressed cell growth, invasiveness and sphere formation

Using the previously developed ENCORI algorithm, we observed the remarkably increased expression of *METTL16* transcript in liver cancer (LIHC) compared with normal samples (Fig. 1A). We also used the online tool Kaplan-Meier Plotter to search for the association of *METTL16* expression with HCC prognosis and found that high expression of *METTL16* foreboded worse overall survival (Fig. 1B). The human protein atlas online resource showed the high expression of METTL16 protein in HCC specimens (Fig. 1C). Validating the online predictions, we collected a cohort of human clinical samples to obtain their RNA and protein extracts. Using quantitative PCR, we obtained evidence for elevated *METTL16* mRNA expression in primary HCC tumors compared with matched healthy samples (Fig. 1D). The Kaplan-Meier survival curve revealed that high *METTL16* expression (above median) predicted poor survival in HCC patients (Fig. 1E). Through immunoblotting, we also confirmed the upregulation of METTL16 protein in HCC tumors compared with adjacent non-cancerous tissues (Fig. 1F). Likewise, expression analysis of METTL16 in HCC cell lines showed elevated METTL16 protein levels in MHCC97, Huh-7, and Hep3B HCC cells relative to normal THLE-2 cells (Fig. 1G). Hence, increased expression of METTL16 observed in HCC is tightly linked to HCC prognosis.

To examine whether upregulation of METTL16 participates in the carcinogenesis of HCC, we sought to reduce its expression to observe the consequences in MHCC97 and Huh-7 HCC cells, which exhibited more significantly upregulated METTL16 (Fig. 1G). For that purpose, three METTL16 siRNAs (si-METTL16#1, si-METTL16#2 or si-METTL16#3) were transfected separately into the two HCC cell lines, and their knockdown efficiencies were validated by immunoblotting (Fig. 2A). Since si-METTL16#1 and si-METTL16#3 had a stronger knockdown efficacy than si-METTL16#2 (Fig. 2A), the two siRNAs were used in the subsequent experiments. After METTL16 depletion, we observed a significant decrease in cell viability and the number of EdU positive cells (Fig. 2B–2D). Conversely, the apoptosis ratio was remarkably higher in METTL16-depleted HCC cells than that in si-NC controls (Fig. 2E). Using transwell assay, we were able to show that METTL16-depleted HCC cells displayed suppressed invasiveness

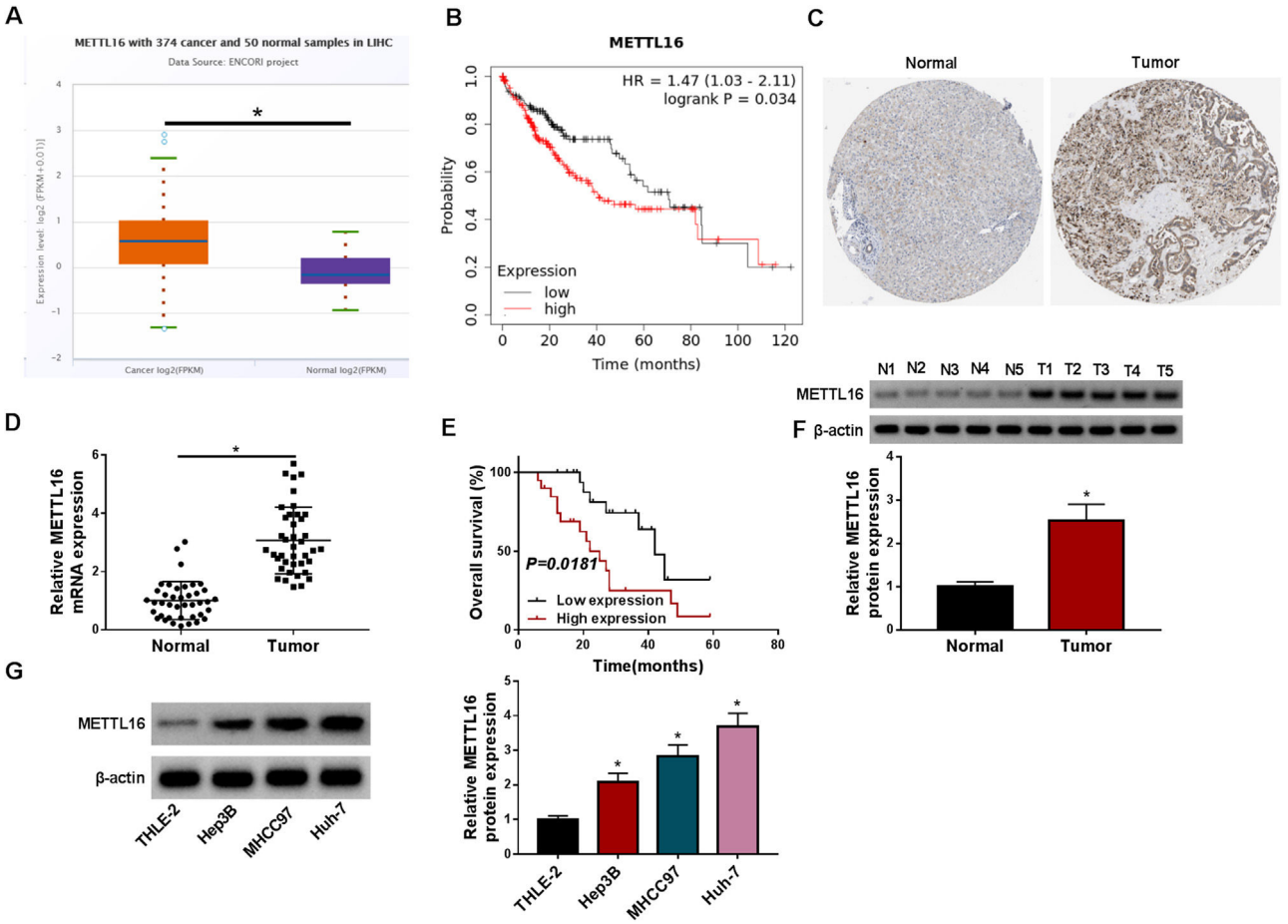

Fig. 1. METTL16 expression is increased in HCC, and elevated METTL16 expression predicts poor HCC prognosis. (A) ENCORI algorithm revealing the upregulation of *METTL16* transcript in liver cancer (LIHC) compared with normal samples. (B) Kaplan-Meier Plotter database showing the association of *METTL16* expression with HCC prognosis. (C) The human protein atlas resource unveiling the high expression of METTL16 protein in HCC specimens. (D) Validation of high *METTL16* transcript in clinical HCC tumors (n = 40) compared with matched healthy samples (n = 40). *P*-value based on the Mann-Whitney U test. (E) Kaplan-Meier survival curve revealing the positive correlation of high *METTL16* expression (above median) with poor survival. *P*-value based on the Log-rank (Mantel-Cox) test. (F) Validation of high METTL16 protein levels in clinical HCC tumors (n = 5) compared with matched healthy samples (n = 5). *P*-value based on a two-tailed Student's *t*-test. (G) Expression of METTL16 protein in MHCC97, Huh-7, and Hep3B HCC cells and non-tumor THLE-2 cells, as evaluated by immunoblotting (n = 3). *P* based on one-way ANOVA followed by Tukey-Kramer *post hoc* test. $^{*}P < 0.05$.

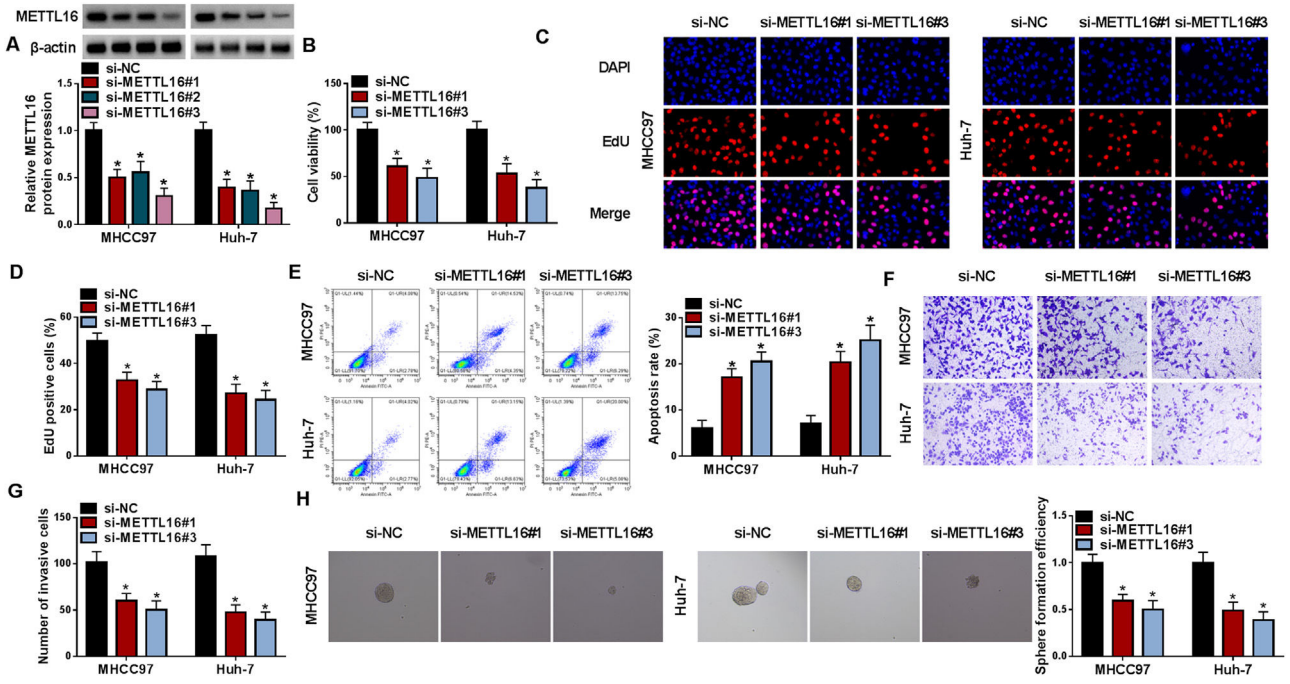

Fig. 2. METTL16 deficiency suppresses HCC cell growth, invasiveness and sphere formation *in vitro*. (A) Expression of METTL16 protein by immunoblotting in MHCC97 and Huh-7 HCC cells transfected with si-NC, si-METTL16#1, si-METTL16#2 or si-METTL16#3. (B-H) MHCC97 and Huh-7 HCC cells were introduced with si-NC, si-METTL16#1, or si-METTL16#3. (B) CCK-8 cell viability assay in transfected MHCC97 and Huh-7 HCC cells. (C and D) EdU cell proliferation assay with MHCC97 and Huh-7 HCC cells transfected as indicated. (E) Flow cytometry for cell apoptosis in MHCC97 and Huh-7 HCC cells after the indicated transfection. (F and G) Transwell invasion assay with thansfected MHCC97 and Huh-7 HCC cells. (H) Sphere formation of MHCC97 and Huh-7 HCC cells after the indicated transfection was assessed. $n = 3$ for A-H. $^*P < 0.05$ based on two-way ANOVA followed by Sidak's multiple comparisons test.

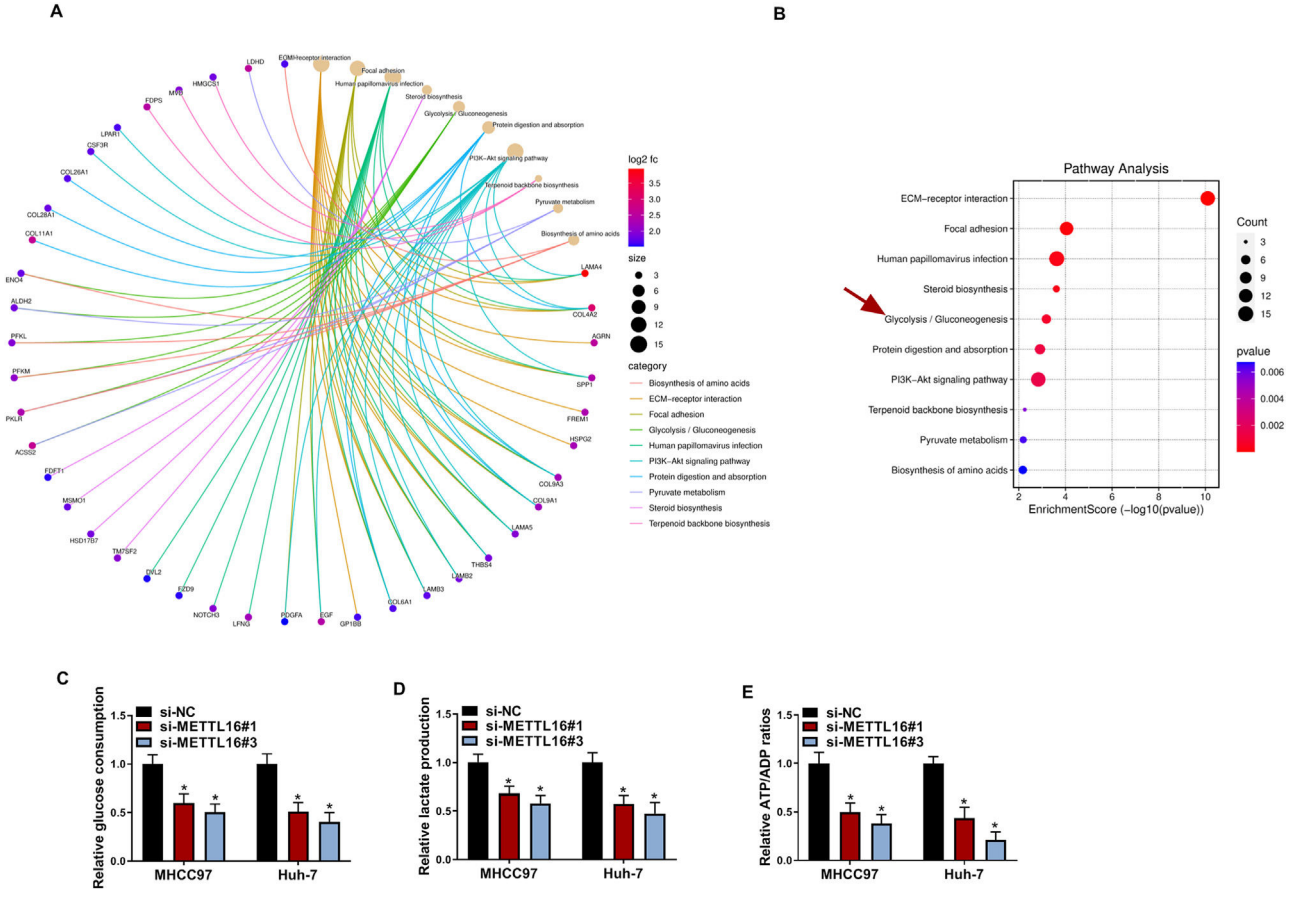

Fig. 3. METTL16 depletion inhibits HCC cell glycolysis *in vitro*. (A and B) GSE224008 dataset revealed many DEGs after METTL16 silencing in Huh-7 liver cancer cells. KEGG pathway enrichment analysis of these DEGs was performed. (C-E) Cell glucose consumption level (C), lactate production level (D), and ATP/ADP ratio (E) in MHCC97 and Huh-7 HCC cells transfected with si-NC, si-METTL16#1, or si-METTL16#3 were evaluated using corresponding assay kits ($n = 3$). *P* based on two-way ANOVA followed by Sidak's multiple comparisons test. $^*P < 0.05$.

(Fig. 2F and 2G). Furthermore, the efficiency of sphere formation of MHCC97 and Huh-7 HCC cells was markedly diminished following METTL16 deficiency (Fig. 2H). Taken together, our results suggest that upregulated METTL16 plays a promoting role in HCC tumorigenesis.

3.2. *Knocking down METTL16 diminishes HCC cell glycolysis* in vitro

In an attempt to evaluate the mechanism behind the action of METTL16 in HCC, we performed a bioinformatic analysis for the downstream targets of METTL16. The GSE224008 dataset revealed many differentially expressed genes (DEGs) after METTL16 silencing in Huh-7 liver cancer cells. Through KEGG pathway enrichment analysis, we found that these DEGs were closely related to various important pathways, including glycolysis/gluconeogenesis pathway (Fig. 3A and 3B). We thus hypothesized that METTL16 might be involved in HCC glycolysis. By applying commercially available assay kits, we found significantly decreased glucose consumption, lactate production, and ATP/ADP ratio in METTL16-silenced MHCC97 and Huh-7 HCC cells compared with si-NC control cells (Fig. 3C–3E). These data imply that upregulated METTL16 may contribute to enhanced glycolysis in HCC.

3.3. *METTL16 mediates m6A methylation to stabilize PFKM mRNA by an IGF2BP3-dependent manner*

After studying the modulation of METTL16 in HCC glycolysis, we next investigated the molecular basis underlying this modulation. Further observation of the GSE224008 dataset showed that PFKM, a crucial rate-limiting enzyme in glycolysis that has been identified as a potential driver in HCC [13], was strongly reduced in METTL16-depleted Huh-7 cells (Fig. 4A). Using mRNA and protein expression analyses, we were able to demonstrate that METTL16 knockdown led

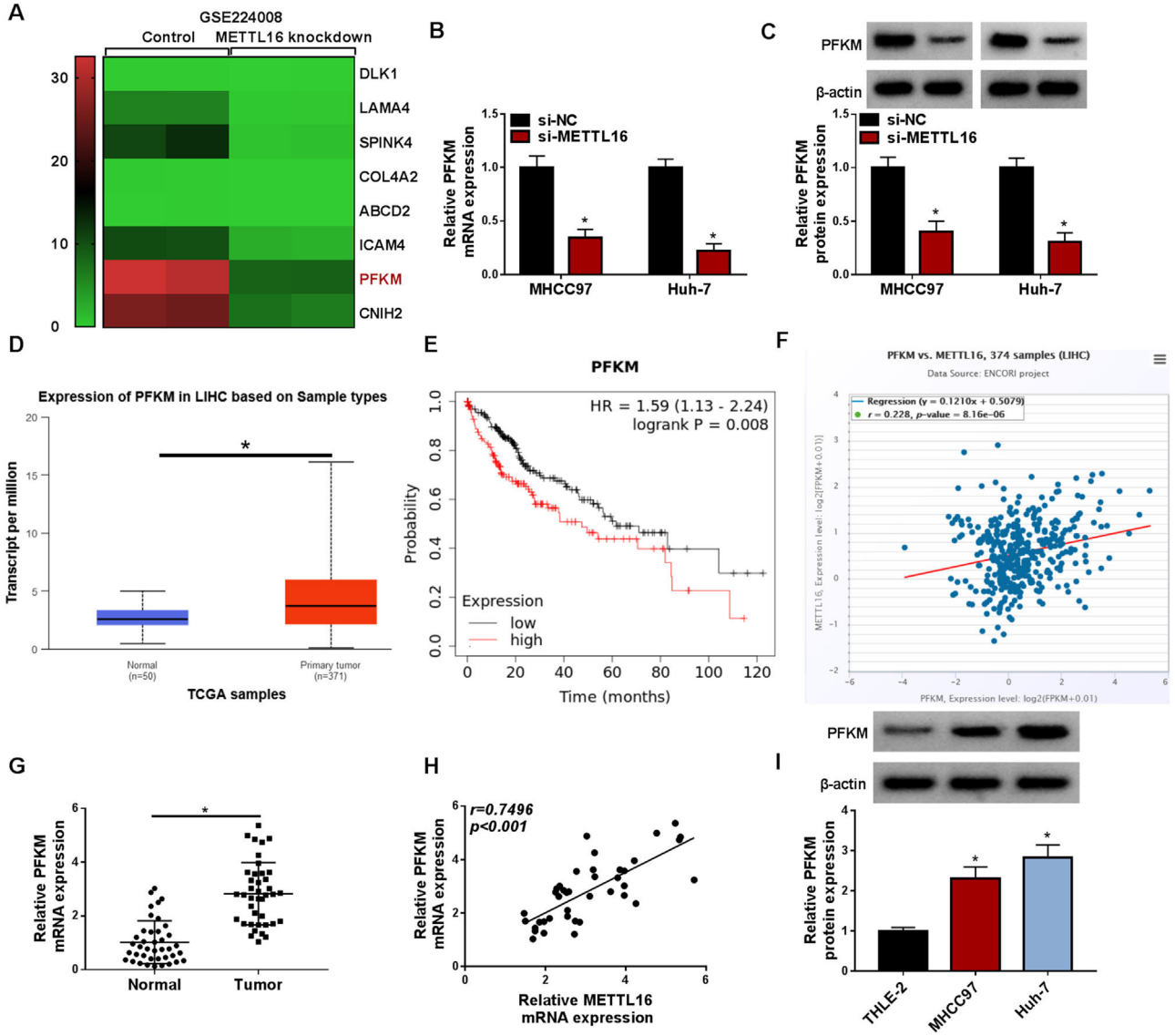

Fig. 4. METTL16 affects PFKM expression in HCC cells. (A) GSE224008 dataset showing the decrease of *PFKM* transcript in Huh-7 liver cancer cells with METTL16 knockdown. (B) Expression of *PFKM* mRNA transcript in MHCC97 and Huh-7 HCC cells transfected with si-NC or si-METTL16 (the 1:1 ratio mix of si-METTL16#1:si-METTL16#3) by quantitative PCR ($n = 3$). *P* based on two-way ANOVA followed by Sidak's multiple comparisons test. (C) Expression of PFKM protein in si-NC- or si-METTL16-transfected HCC cells ($n = 3$). *P* based on two-way ANOVA followed by Sidak's multiple comparisons test. (D) TCGA database showing the high expression of *PFKM* mRNA in liver cancer (LIHC) tissues compared with normal samples. (E) Kaplan-Meier Plotter database predicting the association of *PFKM* expression with HCC prognosis. (F) ENCORI algorithm predicting the positive expression correlation of *PFKM* with *METTL16*. (G) Validation of high *PFKM* mRNA transcript in clinical HCC tumors ($n = 40$) compared with matched healthy samples ($n = 40$). *P*-value based on the Mann-Whitney U test. (H) Validation of the positive expression correlation of *PFKM* with *METTL16* in clinical HCC tumors ($n = 40$) by Pearson's correlation analysis. (I) Expression of PFKM protein in MHCC97, Huh-7, and Hep3B HCC cells and non-tumor THLE-2 cells by immunoblotting ($n = 3$). *P* based on one-way ANOVA followed by Tukey-Kramer *post hoc* test. $^*P < 0.05$.

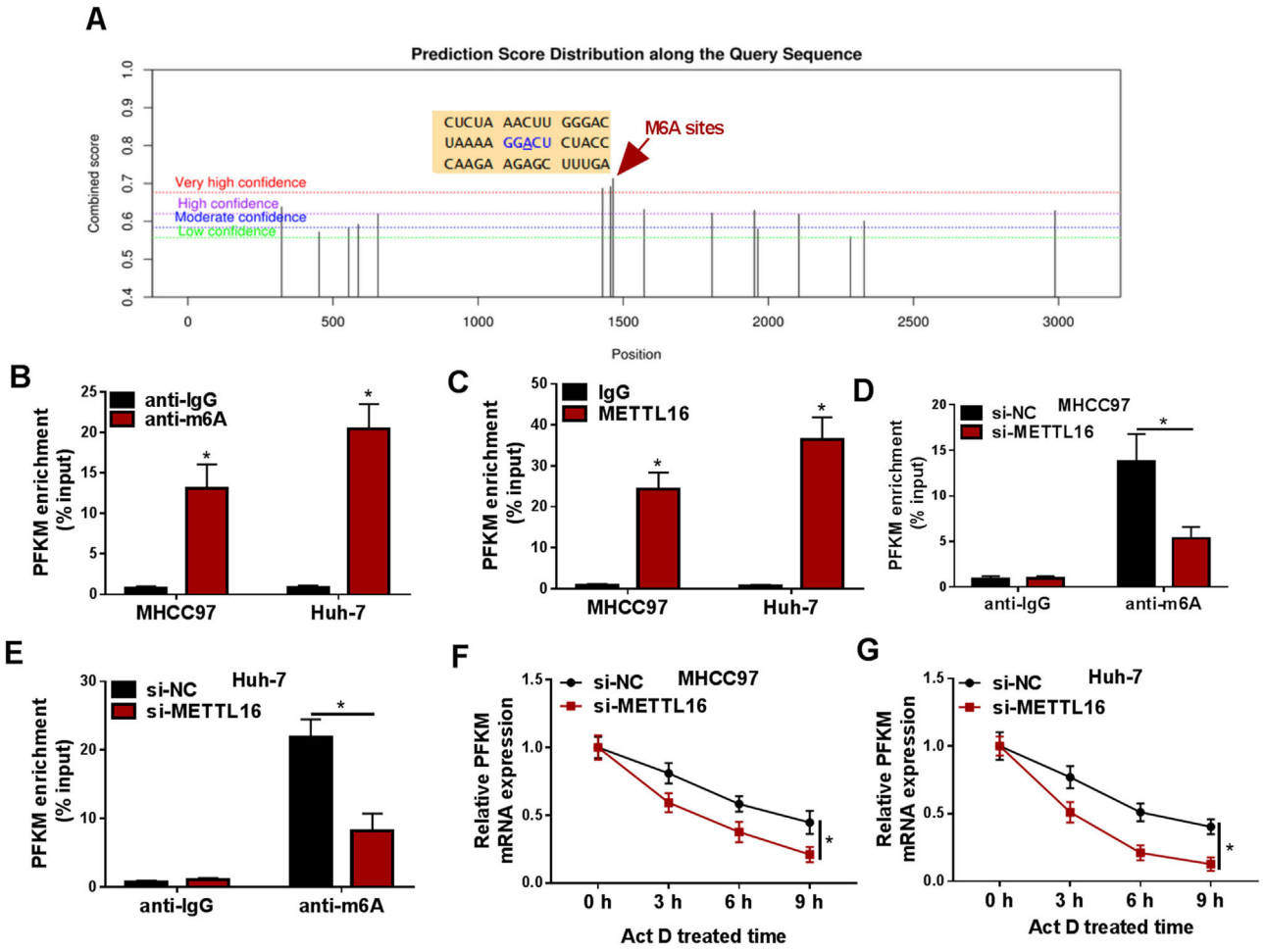

Fig. 5. METTL16 mediates m6A methylation to stabilize *PFKM* mRNA. (A) SRAMP website predicted the putative m6A methylation sites within *PFKM* mRNA. (B and C) MeRIP with anti-m6A antibody (B) and RIP with anti-METTL16 antibody (C) were performed using lysates of MHCC97 and Huh-7 HCC cells. Enrichment of *PFKM* transcript was gauged by quantitative PCR ($n = 3$). (D and E) MeRIP with anti-m6A antibody was done using lysates of si-NC- or si-METTL16-transfected cells, and followed by detection of *PFKM* transcript enrichment by quantitative PCR ($n = 3$). (F and G) Si-NC- or si-METTL16-transfected MHCC97 and Huh-7 cells were subjected to Act D treatment for the indicated time and checked for *PFKM* mRNA levels by quantitative PCR ($n = 3$). $^*P < 0.05$ based on two-way ANOVA followed by Sidak's multiple comparisons test.

to a significant decrease in PFKM expression in MHCC97 and Huh-7 HCC cells (Fig. 4B and 4C). The open-access TCGA database predicted the elevated expression of *PFKM* transcript in liver cancer (Fig. 4D). Elevated *PFKM* levels foreboded worse survival in HCC, examined by the Kaplan-Meier Plotter web (Fig. 4E). In addition, the ENCORI algorithm revealed the possible positive expression correlation of *PFKM* with *METTL16* in liver cancer (Fig. 4F). Using quantitative PCR, we also obtained evidence for the increased expression of *PFKM* mRNA transcript and the positive expression correlation between *PFKM* and *METTL16* in primary HCC tumors (Fig. 4G and 4H). Additionally, using immunoblotting, we observed increased levels of PFKM protein in MHCC97 and Huh-7 HCC cells compared with non-tumor THLE-2 cells (Fig. 4I).

Dysregulation of METTL16, an atypical methyltransferase, has been reported to play a pro-tumorigenic role via an m6A-dependent mechanism [7,14]. Thus, we further studied whether METTL16 affects PFKM expression via the m6A-dependent mechanism. The online website SRAMP predicted the putative m6A methylation sites within *PFKM* mRNA (Fig. 5A). MeRIP experiments using an anti-m6A antibody validated the existence of m6A-modified *PFKM* mRNA in the two HCC cell lines, as presented by the enrichment of *PFKM* mRNA transcript in m6A-associating precipitates (Fig. 5B). RIP experiments using an anti-METTL16 antibody also confirmed the direct relationship of METTL16 with *PFKM* mRNA (Fig. 5C). Furthermore, si-METTL16-mediated METTL16 depletion significantly reduced the levels of m6A-modified *PFKM* mRNA in MHCC97 and Huh-7 cells (Fig. 5D and 5E). Interestingly, using Act D treatment to inhibit transcription, we observed that silencing of METTL16 strongly weakened the stability of *PFKM* mRNA in both HCC cell lines (Fig. 5F and 5G). All these observations demonstrate that METTL16 mediates m6A methylation of *PFKM* mRNA to stability this mRNA transcript.

The knowledge of RNA m6A modification has revealed essential roles of m6A binding proteins (m6A readers) in RNA stability [15]. Therefore, we also performed bioinformatic and experimental analyses to identify an m6A reader associating with the regulation of METTL16 in *PFKM* mRNA stability. Using the online ENCORI algorithm, we observed the putative binding of IGF2BP3, a crucial m6A reader that is reported to stabilize target mRNAs in HCC [16,17], to *PFKM* mRNA (Fig. 6A). The ENCORI algorithm also predicted the positive expression correlation between *PFKM* and *IGF2BP3* in liver cancer (Fig. 6B). The TCGA database showed the upregulation of *IGF2BP3* transcript in liver cancer samples (Fig. 6C), and the Kaplan-Meier Plotter tool revealed that *IGF2BP3* upregulation predicted poor prognosis in this disease (Fig. 6D). The transfection efficiencies of si-IGF2BP3 and IGF2BP3 expression construct were validated by immunoblotting (Fig. 6E). Through quantitative PCR, we demonstrated the positive modulation of IGF2BP3 in *PFKM* mRNA expression in MHCC97 and Huh-7 cells (Fig. 6F). Interestingly, METTL16 depletion

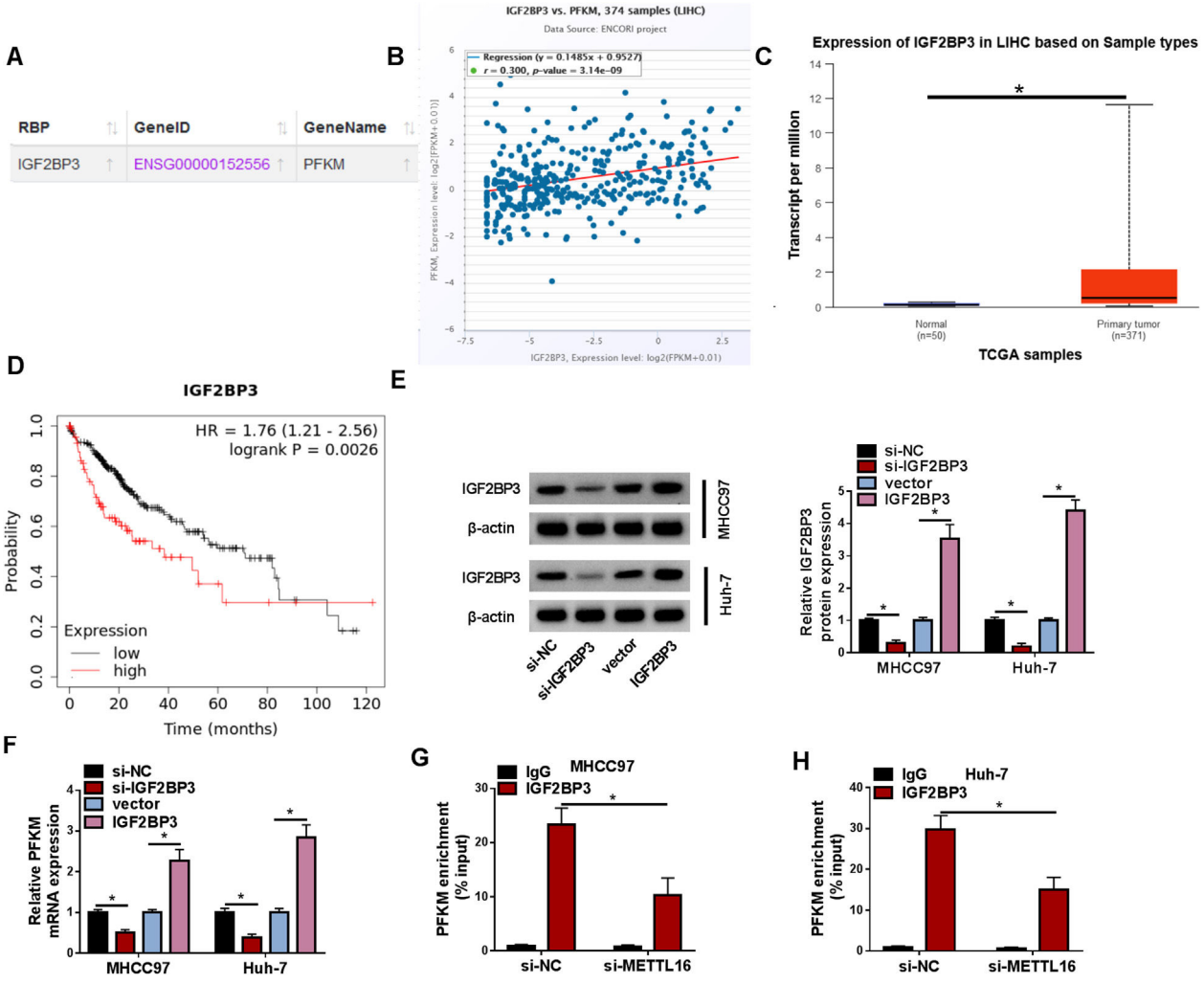

Fig. 6. IGF2BP3 influences *PFKM* mRNA expression. (A) ENCORI algorithm observed the putative binding of IGF2BP3 to *PFKM* mRNA transcript. (B) ENCORI algorithm predicted the positive expression correlation between *PFKM* and *IGF2BP3* in liver cancer (LIHC). (C) TCGA database showed the upregulation of *IGF2BP3* transcript in LIHC samples. (D) Kaplan-Meier Plotter tool revealed that *IGF2BP3* upregulation predicted poor prognosis in LIHC patients. (E) Expression of IGF2BP3 protein in MHCC97 and Huh-7 cells transfected with si-NC, si-IGF2BP3, vector, or IGF2BP3 expression construct (n = 3). P based on two-way ANOVA followed by Sidak's multiple comparisons test. (F) Expression of *PFKM* mRNA in MHCC97 and Huh-7 cells transfected as indicated (n = 3). P based on two-way ANOVA followed by Sidak's multiple comparisons test. (G and H) RIP with anti-IGF2BP3 antibody was done using lysates of si-NC- or si-METTL16-transfected cells, followed by detection of *PFKM* transcript enrichment by quantitative PCR (n = 3). P based on two-way ANOVA followed by Sidak's multiple comparisons test. $^*P < 0.05$.

significantly diminished the relationship of IGF2BP3 with *PFKM* mRNA, as evidenced by the reduction of *PFKM* mRNA enrichment levels in IGF2BP3-associating precipitates (Fig. 6G and 6H). Taking together, we conclude that METTL16 enhances *PFKM* mRNA stability via an IGF2BP3-m6A-dependent manner.

3.4. *Restored PFKM expression has a counteracting effect on METTL16 deficiency-mediated* in vitro *cell phenotype alterations and* in vivo *xenograft growth suppression*

Our findings have established the positive regulation of METTL16 in *PFKM* mRNA stability in HCC cells. Accordingly, we further performed a series of *in vitro* and *in vivo* rescue assays to elucidate whether METTL16 affects HCC carcinogenesis through PFKM. In METTL16-silenced MHCC97 and Huh-7 cells, a PFKM construct was used to elevate PFKM expression (Fig. 7A). Restored PFKM levels significantly reversed METTL16 depletion-mediated cell *in vitro* viability inhibition (Fig. 7B), proliferation suppression (Fig. 7C and 7D), apoptosis promotion (Fig. 7E), invasion repression (Fig. 7F), and sphere formation reduction (Fig. 7G) in MHCC97 and Huh-7 cells. Likewise, PFKM increase strongly counteracted si-METTL16-imposed *in vitro* diminishment of glucose consumption (Fig. 7H), lactate production (Fig. 7I), and ATP/ADP ratio (Fig. 7J) of MHCC97 and Huh-7 cells.

We also performed *in vivo* experiments by generating MHCC97 mouse xenograft tumors accompanied with or without intratumoral administration of the PFKM expression construct. Sh-METTL16-injected mice produced significantly smaller tumors than sh-NC controls (Fig. 8A and 8B). Whereas, administration of the PFKM construct strongly abolished this phenomenon (Fig. 8A and 8B). Sh-METTL16 MHCC97 xenografts exhibited reduced PFKM protein expression, while the PFKM construct reversed the reduction (Fig. 8C and 8D). In addition, xenografts formed by sh-METTL16-infected MHCC97 cells had fewer cells stained for Ki67, and elevated PFKM expression enhanced the number of Ki67 positive tumor cells (Fig. 8D). We then asked whether the METTL16/PFKM axis would result in distant metastasis. At week 6 after cell implantation, H&E staining revealed the occurrence of MHCC97 tumor lung metastasis in sh-NC mice (Fig. 8E). The number of metastatic nodes also supported the occurrence of tumor lung metastasis (Fig. 8F). Sh-METTL16 MHCC97 xenografts displayed decreased lung metastasis, whereas elevated PFKM

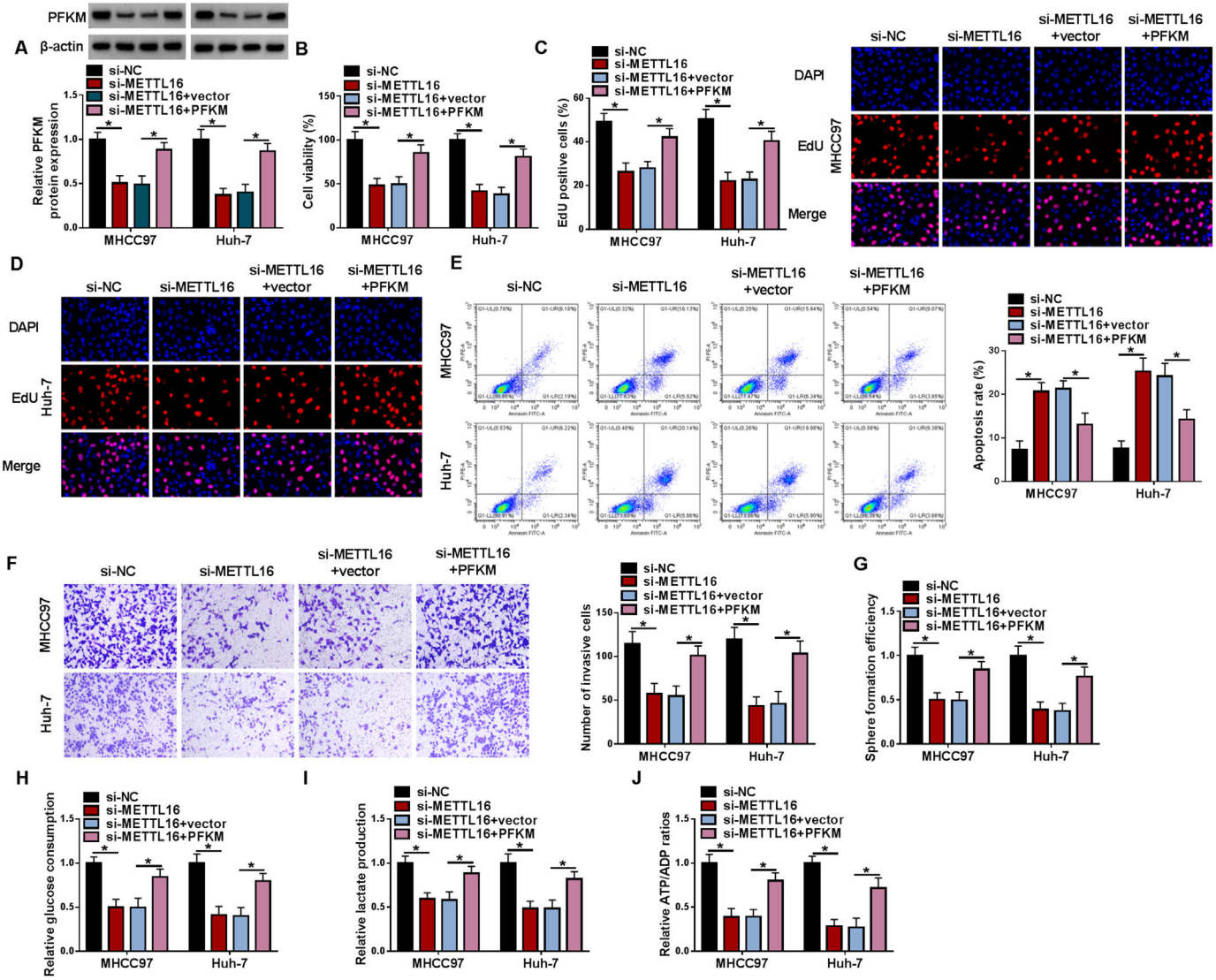

Fig. 7. Restored PFKM expression reverses METTL16 deficiency-mediated cell phenotype alterations *in vitro*. (A-J) MHCC97 and Huh-7 HCC cells were subjected to transfection of si-NC, si-METTL16, si-METTL16+vector, or si-METTL16+PFKM expression construct. (A) Expression of PFKM protein by immunoblotting in transfected cells. (B) CCK-8 cell viability assay in transfected MHCC97 and Huh-7 HCC cells. (C and D) EdU cell proliferation assay with MHCC97 and Huh-7 HCC cells transfected as indicated. (E) Flow cytometry for cell apoptosis in MHCC97 and Huh-7 HCC cells after the indicated transfection. (F) Transwell invasion assay with thansfected MHCC97 and Huh-7 HCC cells. (G) Sphere formation of MHCC97 and Huh-7 HCC cells after the indicated transfection was assessed. (H-J) Cell glucose consumption level, lactate production level, and ATP/ADP ratio in MHCC97 and Huh-7 HCC cells transfected as indicated using corresponding assay kits. $n = 3$ for A-J. $^*P < 0.05$ based on two-way ANOVA followed by Sidak's multiple comparisons test.

expression strongly enhanced MHCC97 tumor lung metastasis (Fig. 8E and 8F). Collectively, we establish the notion that PFKM works as a functional effector of METTL16 in promoting HCC.

3.5. POU3F2 promotes the transcription of METTL16 by binding to the METTL16 promoter

Finally, we also investigated the mechanism underlying METTL16 upregulation in HCC. Dysregulation of transcription factors (TFs) is directly associated with liver tumorigenesis [18]. We therefore decided to elucidate the upstream TFs in promoting *METTL16* transcription using three TF-predicting algorithms (Genecards, PROMO and JASPAR). A total of two putative TFs (YY1 and POU3F2) that overlapped among these algorithms were found (Fig. 9A). The depletion efficacy of si-YY1 or si-POU3F2 was confirmed by immunoblotting in HCC cells (Fig. 9B and 9C). Interestingly, the expression of *METTL16* mRNA transcript was markedly decreased after depletion of YY1 or POU3F2 in Huh-7 cells (Fig. 9D). Because of the more significantly reduction by si-POU3F2 (Fig. 9D), we focused on POU3F2 in the present work. The JASPAR algorithm predicted the putative binding sites (TTAAGCAAATTG) for POU3F2 in the *METTL16* promoter (Fig. 9E). ChIP experiments with an anti-POU3F2 antibody validated the relationship of POU3F2 with the *METTL16* promoter (Fig. 9F). To examine the modulation of POU3F2 in *METTL16* transcription via the target region, we generated *METTL16* promoter reporter constructs containing the putative binding sequence (WT-METTL16) or mutant target region (MUT-METTL16). Luciferase assays showed that si-POU3F2-driven POU3F2 depletion strongly reduced the luciferase activity of WT-METTL16, but not MUT-METTL16 (Fig. 9G and 9H). In addition, in clinical HCC samples, *POU3F2* expression was enhanced and positively related to *METTL16* expression (Fig. 9I and 9J). Further observation of the influence of POU3F2 in METTL16 expression confirmed that POU3F2 silencing led to a significant reduction in METTL16 protein expression (Fig. 9K). These results demonstrate that upregulated POU3F2 is a contributor to METTL16 increase by enhancing METTL16 transcription in HCC.

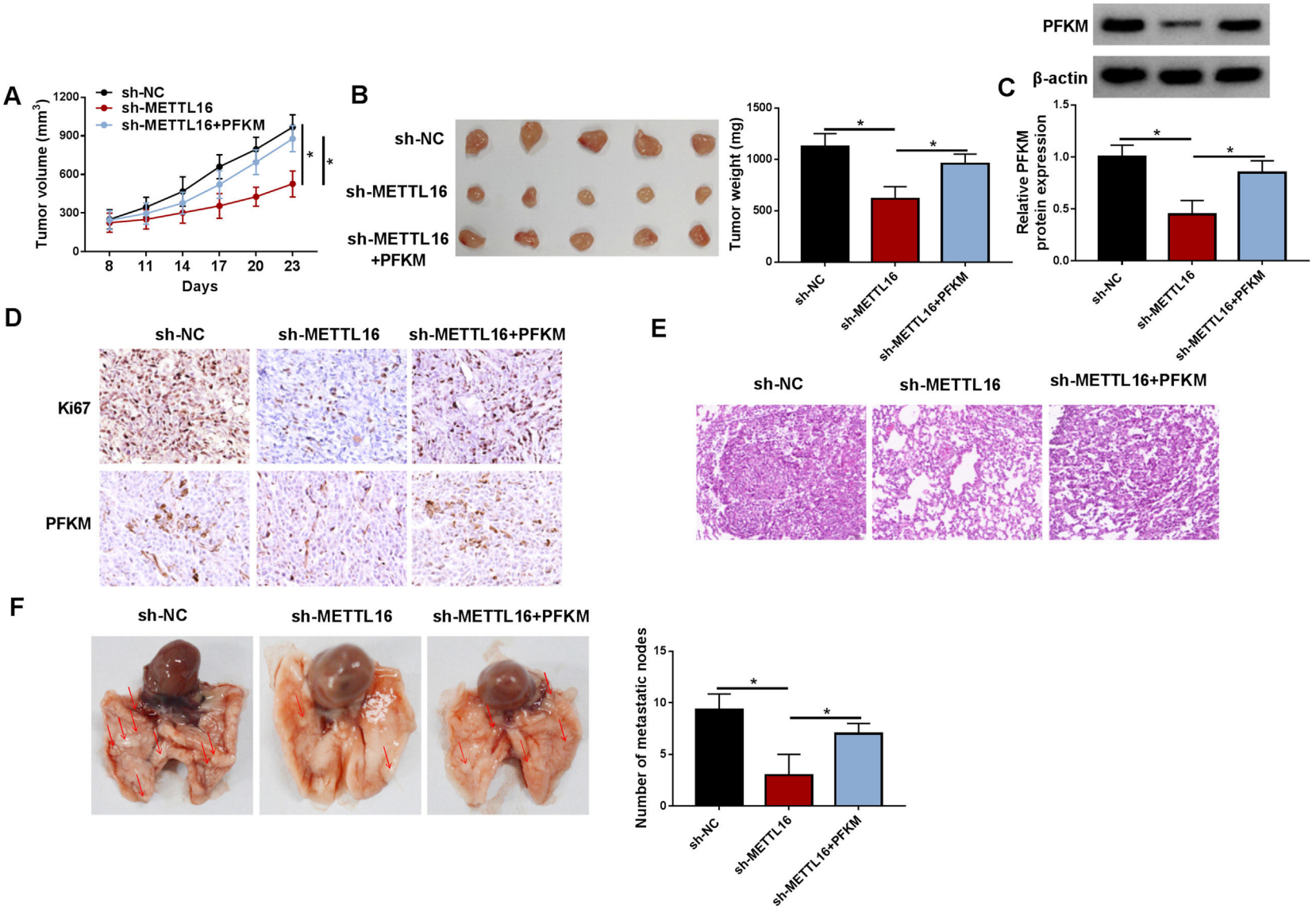

Fig. 8. Restored PFKM expression abolishes METTL16 deficiency-driven tumor growth suppression *in vivo*. Sh-NC- or sh-METTL16 lentivirus-infected MHCC97 cells were implanted subcutaneously or intravenously into nude mice, with or without administration of the PFKM expression lentivirus. $n = 8$ for each group. Five mice were used for xenograft collection at day 23, and three mice were used for lung collection at week 6. (A) Growth curves of MHCC97 xenografts. (B) Images and mean weight of MHCC97 xenografts on day 23. (C) Expression of PFKM protein by immunoblotting in MHCC97 xenografts. (D) Expression of PFKM and Ki67 by immunohistochemistry in MHCC97 xenografts. (E) H&E staining of lung tissues of xenograft mice. (F) The number of metastasis nodes in lung tissues of xenograft mice. $^*P < 0.05$ based on one-way ANOVA followed by Tukey-Kramer *post hoc* test.

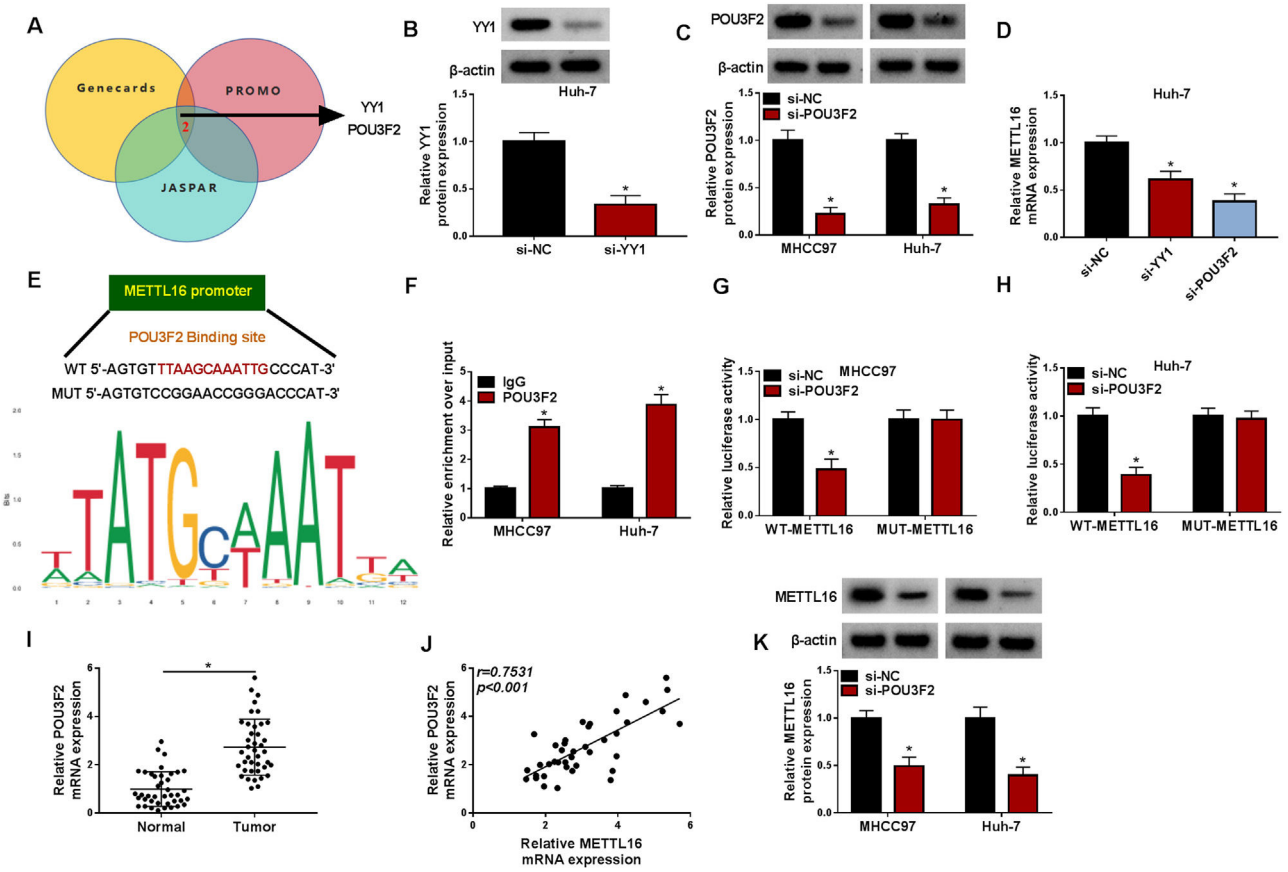

Fig. 9. POU3F2 enhances *METTL16* transcription in HCC cells. (A) Genecards, PROMO and JASPAR algorithms predicted the putative TFs in regulating METTL16 transcription. (B and C) The transfection efficiencies of si-YY1 or si-POU3F2 were confirmed by immunoblotting. *P*-value based on a two-tailed Student's *t*-test or two-way ANOVA followed by Sidak's multiple comparisons test. (D) Expression of *METTL16* transcript in Huh-7 cells after depletion of YY1 or POU3F2. *P* based on one-way ANOVA followed by Tukey-Kramer *post hoc* test. (E) JASPAR algorithm predicted the putative binding sites between POU3F2 and the *METTL16* promoter. (F) ChIP with an anti-POU3F2 antibody was done using lysates of MHCC97 and Huh-7 cells. *P* based on two-way ANOVA followed by Sidak's multiple comparisons test. (G and H) Luciferase assays in cells transfected with si-POU3F2 or si-NC and WT-METTL16 or MUT-METTL16. *P* based on two-way ANOVA followed by Sidak's multiple comparisons test. (I) Validation of high *POU3F2* mRNA transcript in clinical HCC tumors ($n = 40$) compared with matched healthy samples ($n = 40$). *P*-value based on the Mann-Whitney U test. (J) Validation of the positive expression correlation of *POU3F2* with *METTL16* in clinical HCC tumors ($n = 40$) by Pearson's correlation analysis. (K) Expression of METTL16 protein in cells after transfection with si-POU3F2 or si-NC. *P* based on two-way ANOVA followed by Sidak's multiple comparisons test. $^*P < 0.05$.

4. Discussion

Advanced therapies are beneficial to early stage HCC and fail to provide great benefit for HCC at the advanced stage. Thus, investigating the molecular pathogenesis of HCC is crucial for developing innovative therapeutic approaches against HCC. Being the second methyltransferase identified, m6A writer METTL16 is aberrantly expressed in various cancers, and its deregulation is strongly linked to human carcinogenesis [19]. Recent work has documented the pro-tumorigenic role of METTL16 in HCC through an m6A-dependent mode [9,10,20]. Consistently, our findings provide support to the fact that increased METTL16 levels observed in HCC are tightly related to HCC prognosis, and METTL16 plays a promoting role in HCC tumorigenesis. Increased glycolysis in cancer cells contributes to oncogenesis and cancer progression. Modulation of glycolysis has been proposed for improving cancer treatment [4]. Our results also show that depletion of METTL16 results in suppressed glycolysis in HCC cells. Hence, METTL16 inhibitors may offer the potential opportunity to combat HCC.

As a crucial regulatory enzyme in glycolysis, PFKM is capable of enhancing glycolysis and thus exerts a promoting impact on human tumorigenesis [21]. An important example is that mutation of PFKM has been described to hinder cancer cell proliferation, xenograft growth and metastasis in ovarian cancer [22]. YTHDC1-mediated *PFKM* mRNA m6A methylation takes part in osteosarcoma pathogenesis by modulating glycolysis [23]. Furthermore, PFKM is implicated in HCC cell growth and glycolysis [24]. Elevated expression of PFKM contributes to enhanced glycolysis, growth, and invasiveness in HCC cells [13]. These reports suggest the oncogenic effect of PFKM on human malignancies, including HCC. Here, we have found the positive modulation of METTL16 in PFKM expression. Moreover, METTL16 can mediate m6A methylation to stabilize *PFKM* mRNA. IGF2BP3, a key m6A reader, functions as a critical player in HCC by upgrading target mRNA stability [16,17]. Importantly, we demonstrate, for the first time, that METTL16-mediated *PFKM* mRNA stabilization is IGF2BP3-dependent in HCC cells. Through *in vitro* and *in vivo* rescue assays, we define that PFKM has the ability to work as a functional effector of METTL16 in promoting HCC.

Epigenetic deregulation plays a pro-tumorigenic role that participates in liver carcinogenesis [25]. In this paper, we further highlight an epigenetic event driving METTL16 upregulation in HCC. Considering the crucial functions of TFs in gene expression, we uncover that TF POU3F2 promotes the transcription of *METTL16* in HCC cells. POU3F2 has been identified that operates as a potent oncogenic factor in many types of human malignancies, such as breast cancer, prostate cancer and glioblastoma [26–28]. Moreover, the promoting role of POU3F2 in HCC has been established by previously reported literature [29]. Hence, it appears that POU3F2 upregulates METTL16 to promote HCC development. Nonetheless, additional studies are

needed to further explain the details of the cascade in promoting HCC progression.

With these observations, the si-METTL16 or sh-METTL16 construct appears to represent a highly promising candidate for anti-HCC therapy. It exhibits a dual mechanism of action, not only inhibiting the growth and invasive capabilities of HCC cells but also effectively blocking their glycolysis potential. We envision that METTL16 inhibitors could serve as a pivotal starting point for the development of molecularly targeted therapies against HCC. More studies are required to assess the safety, long-term effectiveness, and potential of such agents in diverse experimental models.

5. Conclusions

In conclusion, we provide novel evidence for the pro-tumorigenic role of METTL16 in HCC. We propose METTL16-mediated *PFKM* mRNA stability via IGF2BP3 as a mechanism by which METTL16 promotes HCC progression, and we further define that TF POU3F2 drives METTL16 upregulation. Our findings highlight the implication of the POU3F2/METTL16/PFKM axis in HCC pathogenesis. Targeting the novel axis represents the potential opportunity to combat HCC.

Funding

This work was supported by Hunan Provincial Health Commission guiding project (No.D202303039177).

Author contributions

All authors contributed significantly to this work. Their contributions include the conceptualization of the study, experimental design, data collection, and analysis. The authors also participated in the drafting and critical revision of the manuscript for important intellectual content. Additionally, all authors have reviewed and approved the final version of the manuscript and agree to be accountable for all aspects of the work, ensuring its accuracy and integrity.

Declaration of interests

The authors declare that they have no conflicts of interest.

References

[1] Bray F, Laversanne M, Sung H, Ferlay J, Siegel RL, Soerjomataram I, Jemal A. Global cancer statistics 2022: GLOBOCAN estimates of incidence and mortality worldwide for 36 cancers in 185 countries. CA Cancer J Clin 2024;74(3):229–63.
[2] Vogel A, Meyer T, Sapisochin G, Salem R, Saborowski A. Hepatocellular carcinoma. Lancet 2022;400(10360):1345–62.
[3] Yuguang Y, Hui T, Cong M, Xin Z, Jiawen K, Yunqiang T. Analysis of the Safety and Effectiveness of Lenvatinib + TACE-HAIC + PD-1 Inhibitor for Intermediate and Advanced Hepatocellular Carcinoma. Lett Drug Des Discov 2024;21(11):2035–45.
[4] Chelakkot C, Chelakkot VS, Shin Y, Song K. Modulating Glycolysis to Improve Cancer Therapy. Int J Mol Sci 2023;24(3).
[5] An Y, Duan H. The role of m6A RNA methylation in cancer metabolism. Mol Cancer 2022;21(1):14.
[6] Satterwhite ER, Mansfield KD. RNA methyltransferase METTL16: targets and function. Wiley Interdiscip Rev RNA 2022;13(2):e1681.
[7] Han L, Dong L, Leung K, Zhao Z, Li Y, Gao L, Chen Z, Xue J, Qing Y, Li W, et al. METTL16 drives leukemogenesis and leukemia stem cell self-renewal by reprogramming BCAA metabolism. Cell Stem Cell 2023;30(1):52–68 .e13.
[8] Wang XK, Zhang YW, Wang CM, Li B, Zhang TZ, Zhou WJ, Cheng LJ, Huo MY, Zhang CH. He YL: METTL16 promotes cell proliferation by up-regulating cyclin D1 expression in gastric cancer. J Cell Mol Med 2021;25(14):6602–17.
[9] Dai YZ, Liu YD, Li J, Chen MT, Huang M, Wang F, Yang QS, Yuan JH, Sun SH. METTL16 promotes hepatocellular carcinoma progression through downregulating RAB11B-AS1 in an m(6)A-dependent manner. Cell Mol Biol Lett 2022;27(1):41.
[10] Wang Y, Yang Y, Yang Y, Dang Y, Guo Z, Zhuang Q, Zheng X, Wang F, Cheng N, Liu X, et al. Hypoxia induces hepatocellular carcinoma metastasis via the HIF-1α/METTL16/lnc-CSMD1-7/RBFOX2 axis. iScience 2023;26(12):108495.
[11] Lee YJ, Shin KJ, Jang HJ, Ryu JS, Lee CY, Yoon JH, Seo JK, Park S, Lee S, Je AR, et al. GPR143 controls ESCRT-dependent exosome biogenesis and promotes cancer metastasis. Dev Cell 2023;58(4):320–34 .e328.
[12] Schampel A, Volovitch O, Koeniger T, Scholz CJ, Jörg S, Linker RA, Wischmeyer E, Wunsch M, Hell JW, Ergün S, et al. Nimodipine fosters remyelination in a mouse model of multiple sclerosis and induces microglia-specific apoptosis. Proc Natl Acad Sci USA 2017;114(16):E3295–304.
[13] Zhou Y, Lin F, Wan T, Chen A, Wang H, Jiang B, Zhao W, Liao S, Wang S, Li G, et al. ZEB1 enhances Warburg effect to facilitate tumorigenesis and metastasis of HCC by transcriptionally activating PFKM. Theranostics 2021;11(12):5926–38.
[14] Sun L, Zhang Y, Yang B, Sun S, Zhang P, Luo Z, Feng T, Cui Z, Zhu T, Li Y, et al. Lactylation of METTL16 promotes cuproptosis via m(6)A-modification on FDX1 mRNA in gastric cancer. Nat Commun 2023;14(1):6523.
[15] Shi H, Wei J. He C: where, when, and how: context-dependent functions of RNA methylation writers, readers, and erasers. Mol Cell 2019;74(4):640–50.
[16] Xu X, Wu S, Zhang Y, Fan W, Lin X, Chen K, Lin X. m6A modification of VEGFA mRNA by RBM15/YTHDF2/IGF2BP3 contributes to angiogenesis of hepatocellular carcinoma. Mol Carcinog 2024.
[17] Hu Z, Chen G, Zhao Y, Gao H, Li L, Yin Y, Jiang J, Wang L, Mang Y, Gao Y, et al. Exosome-derived circCCAR1 promotes CD8 + T-cell dysfunction and anti-PD1 resistance in hepatocellular carcinoma. Mol Cancer 2023;22(1):55.
[18] Gong Z, Yu J, Yang S, Lai PBS, Chen GG. FOX transcription factor family in hepatocellular carcinoma. Biochimica et biophysica acta Reviews on cancer 2020;1874(1):188376.
[19] Qi YN, Liu Z, Hong LL, Li P, Ling ZQ. Methyltransferase-like proteins in cancer biology and potential therapeutic targeting. J Hematol Oncol 2023;16(1):89.
[20] Wang J, Xiu M, Wang J, Gao Y, Li Y. METTL16-SENP3-LTF axis confers ferroptosis resistance and facilitates tumorigenesis in hepatocellular carcinoma. J Hematol Oncol 2024;17(1):78.
[21] Jourdain AA, Begg BE, Mick E, Shah H, Calvo SE, Skinner OS, Sharma R, Blue SM, Yeo GW, Burge CB, et al. Loss of LUC7L2 and U1 snRNP subunits shifts energy metabolism from glycolysis to OXPHOS. Mol Cell 2021;81(9):1905–19 e1912.
[22] Gao W, Huang M, Chen X, Chen J, Zou Z, Li L, Ji K, Nie Z, Yang B, Wei Z, et al. The role of S-nitrosylation of PFKM in regulation of glycolysis in ovarian cancer cells. Cell Death Dis 2021;12(4):408.
[23] Mei Z, Shen Z, Pu J, Liu Q, Liu G, He X, Wang Y, Yue J, Ge S, Li T, et al. NAT10 mediated ac4C acetylation driven m(6)A modification via involvement of YTHDC1-LDHA/PFKM regulates glycolysis and promotes osteosarcoma. Cell Commun Signal 2024;22(1):51.
[24] Fang Y, Tang W, Qu S, Li Z, Zhang X, Miao Y, Zeng Z, Huang H. RBBP7, regulated by SP1, enhances the Warburg effect to facilitate the proliferation of hepatocellular carcinoma cells via PI3K/AKT signaling. J Transl Med 2024;22(1):170.
[25] Nagaraju GP, Dariya B, Kasa P, Peela S, El-Rayes BF. Epigenetics in hepatocellular carcinoma. Semin Cancer Biol 2022;86(Pt 3):622–32.
[26] Zhang H, Zheng J, Fu Y, Ling J, Liu Z, Lin X, Dong X, Sun Y, Tan T, Guo Z, et al. Overexpression of POU3F2 promotes radioresistance in triple-negative breast cancer via Akt pathway activation. Breast Cancer Res Treat 2023;198(3):437–46.
[27] Zhang Z, Zhou C, Li X, Barnes SD, Deng S, Hoover E, Chen CC, Lee YS, Zhang Y, Wang C, et al. Loss of CHD1 Promotes Heterogeneous Mechanisms of Resistance to AR-Targeted Therapy via Chromatin Dysregulation. Cancer cell 2020;37(4):584–98 .e511.
[28] Cui T, Bell EH, McElroy J, Liu K, Sebastian E, Johnson B, Gulati PM, Becker AP, Gray A, Geurts M, et al. A Novel miR-146a-POU3F2/SMARCA5 Pathway Regulates Stemness and Therapeutic Response in Glioblastoma. Mol CancerMol Cancer Res 2021;19(1):48–60.
[29] Fan W, Chen L, Wu X, Zhang T. Circ_0031242 Silencing Mitigates the Progression and Drug Resistance in DDP-Resistant Hepatoma Cells by the miR-924/POU3F2 Axis. Cancer Manag Res 2021;13:743–55.